THE PARAMETERIZATION OF DEEP CONVECTION

ALAN K. BETTS
Atmospheric Research
R.D. 3, Box 3125
Pittsford, VT 05763
akbetts@aol.com

Abstract Insights into the parameterization of convection from two decades of diagnostic studies are reviewed. The life cycle of a convective mesosystem mass flux is described using day 245 from the GARP Atlantic Tropical Experiment as example. The thermodynamic differences between non-precipitating convection and precipitating convection are discussed, as well as the importance of the mid-tropospheric freezing level in the tropics and the saturation pressure budget in the tropics. The strengths and weaknesses of the mass flux representation of deep convection is discussed. Diagnostic studies, which have identified three key vertical modes in the convective heating and drying structure, are outlined. Two are related deep modes associated with precipitation and deep tropospheric ascent, but a variable upward equivalent potential temperature (θ_E) flux. The other is a double mode structure with ascent in the upper troposphere over descent in the lower troposphere, coupled to inflow at the freezing level, with no net precipitation or transport of θ_E; the mode associated with deep mesoscale anvils. We discuss the mass flux formulation of convective updrafts and downdrafts. We outline the concepts (but not the details) behind the Betts-Miller parameterization and suggest two extensions. One is a formulation of the adjustment time in terms of grid-scale and gravity-wave propagation speed for the two primary modes. The second is an explicit parameterization of the mesoscale anvil mode.

1. Introduction

There have been several reviews of convective parameterization in large-scale models including Betts [1], Frank [2], text-books such as Cotton and Anthes [3] and Emanuel [4], and particularly the recent American Meteorological Society monograph by Emanuel and Raymond [5]. This includes a discussion of the Betts-Miller scheme [6], which includes a formulation for unsaturated downdrafts driven by convection. Although I shall summarize the basis of the Betts-Miller scheme in section 4, and suggest a further extension, I will not discuss the details. For the most part, I shall review here some of the fundamental issues that have been uncovered by many researchers over the last twenty-five years; and try to reduce them to their simplest form. As a result this paper is part history, part review and part reinterpretation, together with a few suggestions for a way forward. This paper discusses only the energy and water transports by convection, not the issues of the momentum and

R. K. Smith (ed.), The Physics and Parameterization of Moist Atmospheric Convection, 255–279.

vorticity transports. I only address the closure problem in the limited case of the Betts-Miller scheme in section 4

2. Deep Cumulus Diagnostic results

2.1 DEVELOPMENT OF CUMULUS PARAMETERIZATIONS

The development of cumulus parameterizations, which had started in the 1960's with the work of Kuo [7] and Manabe and Strickler [8] and two important conceptual papers by Ooyama [9] [10], received a stimulus from diagnostic models in the 1970's. The Arakawa and Schubert [11] paper and the diagnostic study of Yanai et al. [12], using data over the tropical Pacific, were closely interlinked. Their cloud model based on entraining updrafts has dominated this school of cumulus parameterization up to this date. They showed how the θ_E flux could be calculated, independent of the precipitation, using this cloud mass flux model. Subsequently this model has been extended to include convective downdrafts Arakawa and Cheng [13]. At the same time as [11][12], there were two parallel papers by Betts [14] [15]. The first [14] introduced the mixed layer model for the dry boundary layer and the subcloud layer, which was included in the Arakawa-Schubert parameterization. This paper also extended the use of conserved variables (in particular, the liquid water potential temperature, dealing with the coupling of the enthalpy and liquid water fluxes in convection), and discussed the concept of lapse rate equilibrium for shallow convection. The second paper [15] used data from the first Venezuela International Meteorological and Hydrological Experiment (VIMHEX) to formulate an updraft-downdraft budget model for mesoscale cumulonimbus systems, based on compositing rawinsonde observations in relation to radar echos. It showed how using θ_E conservation *separately* for the updraft and

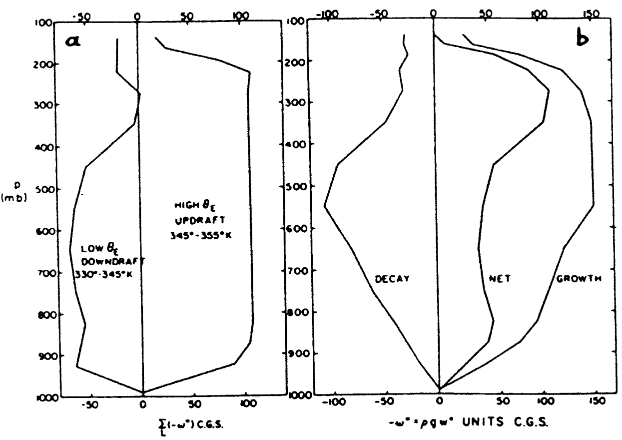

Figure 1a. Vertical mass fluxes for high and low θ_E ranges showing simplified bulk updraft and downdraft (from Betts, 1973b). The peak mass flux of 150 (archaic) CGS units corresponds to 1.5 kg m^{-2} s^{-1} over a 25 km diameter echo for a time interval of 66 minutes.

Figure 1b. As Fig. 1a for vertical mass flux, partitioned into growth and decay phases, together with the life-cycle mean mass flux.

downdraft circulations permitted a separate evaluation of updraft condensation, evaporation into the downdraft, and net precipitation. Figure 1a shows the mass fluxes associated with the high θ_E updraft circulation and the low θ_E downdraft circulation. The paper concluded that half the condensation in the updraft was evaporated into the downdrafts. The composite mesoscale system was also partitioned temporally into the growth and decay phase (Figure 1b). This showed how the net lifecycle upward mass flux was the resultant of an *upward* mass circulation in the growth phase, and a *downward* circulation in the decay phase. The paper also showed that the low level transformation by deep convection was dominated by cold dry downdraft outflows. The data used by [15] was quite primitive, but the subsequent tropical field programs have supported the conclusions of the analysis. The second VIMHEX experiment explored in more detail the transports by unsaturated downdrafts [16] and their modeling (Betts and Silva Dias [17]). Miller and Betts [18] used a mesoscale model to study the distinction between convective and mesoscale downdrafts, reaching similar conclusions to pioneering papers by Zipser [19] [20] and the GATE squall-line study of Houze [21].

2.2. GATE DIAGNOSTIC STUDIES

By the end of that decade, it was clear from these tropical studies over land and from the Global Atmospheric Research Program (GARP) Atlantic Tropical Experiment (GATE) (see reviews by Betts [22]; Houze and Betts [23]) that parameterizing tropical convection needed a model for the lifecycle effect of mesoscale complexes, which evolve from lines of cumulonimbus to mesoscale anvil systems within 6-12 hours, on horizontal scales that are not well resolved in global models.

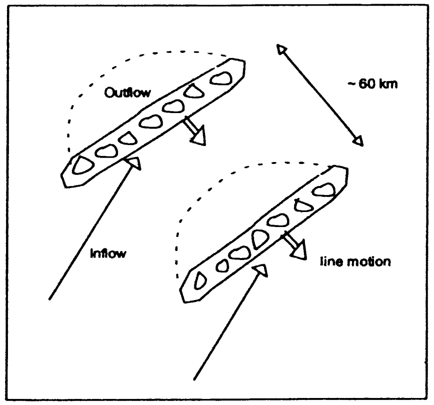

Figure 2. Schematic of GATE convective band development.

Figure 2 is a schematic, typical of the GATE environment with strong shear in the low levels. Within the time-span of a typical mesoscale aircraft mission, the observer would see the development of cumulonimbus bands oriented along the low level shear, with inflows on one side and a developing anvil outflow to the rear. A typical spacing might be 60 km. As each line evolved, the strong convection would decay, and a deep mesoscale anvil would persist often for many hours, with steady stratiform rain and a characteristic bright band at the freezing level (Leary and Houze [24] [25] [26]). On some occasions, faster moving cross-shear lines with trailing anvils, and some of the characteristics of squall-lines, were observed (Barnes and Sieckman, [27]). It was also clear from the detailed analyses of Ooyama in the late 1970's, that the freezing level, which in the tropics is in the mid-troposphere, is dynamically significant. In the mesoscale anvil stage, it is the level of maximum convergence, with ascent above in the region of condensation and freezing, and descent below driven by the evaporation and melting of falling precipitation. However, although the analysis theory was published later in Ooyama [28], only some of the fascinating lifecycle case studies have been fully published. (The Ooyama, Chu and Esbensen wind and thermodynamic analyses are available in an archive at the National Center for Atmospheric Research: documentation is available in Esbensen and Ooyama [29].) Tollerud and Esbensen [30] and Esbensen et al. [31] published some composites of mass, heat and moisture budgets of non-squall clusters based on that data. Other GATE composites were published (Frank [32], Johnson [33]), based on larger scale analyses, but they do not show the mesoscale lifecycles well, because of the smoothing involved in the compositing. The interpretation of diagnostic budgets by Johnson [34] in terms of convective and mesoscale components was however a significant step forward. The most detailed analysis of the Ooyama, Chu and Esbensen dataset was published by Cheng [35] [36] and Cheng and Yanai [37]. Using an Arakawa-Schubert type cloud model with a spectrum of entraining updrafts and downdrafts, together with a mesoscale circulation, Cheng [35] first explored a tilted updraft model, and then systematically determined mass flux distributions for convective-scale updrafts and downdrafts. Cheng and Yanai [37] used the results from the cloud model to extract a mesoscale mass flux and heating function, which explicitly show the mesoscale couplet of heating and drying over cooling and moistening for several GATE cloud clusters. I will return to their analysis in section 3.7.

2.3. GATE CLOUD CLUSTER LIFECYCLE ON DAY 245

As a brief review, I will present an example here for the life cycle mass flux evolution of a major GATE cloud cluster on Julian Day 245. In the published literature, Betts [22] gave a preliminary analyses of the mass flux evolution for this day; Mower et al. [38] analyzed the synoptic, radar and aircraft data for this day, and Warner [39] analyzed the cloud fields. This cluster evolution is an excellent example, as it occurred over the GATE ship array, and the evolution can be seen in both time and space. Bands of convection developed during the day, evolved into a mesoscale complex and then decayed. The daytime evolution over the ship array was studied by a stack of five aircraft [38]; for which the present author was the airborne mission scientist. This cluster is case 31 in [37].

Figure 3 shows a time-series (from the Ooyama analysis) of the mean vertical motion, ω, from 0300 UTC to 2400 UTC on September 2, 1994 (Julian Day 245) at 3 hour intervals at 8.5°N, 22°W, just east of the center of the GATE ship array. The mass field shows upward vertical motion initially peaking in the lower troposphere at 0300 UTC. By noon there was a strong ascent through the whole troposphere with the peak vertical motion in the middle troposphere. Then the upward motion strengthens further in the upper troposphere (1500 and 1800 UTC), as it decays in the lower troposphere. This is the stage when strong mesoscale ascent develops in the extensive anvils in the upper troposphere, and underneath a mesoscale downdraft forms, driven by the melting and evaporation of falling precipitation.

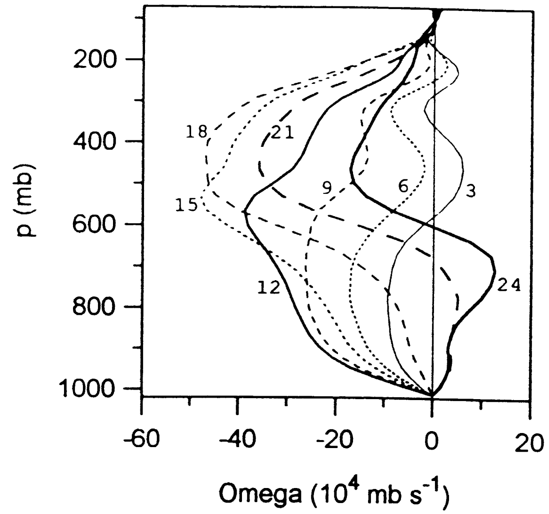

Figure 3. Time-series of the mean vertical motion at 8.5°N, 22°W from 0300-2400 UTC on September 2 1974 (Day 245), from Ooyama's analysis of GATE wind sounding data.

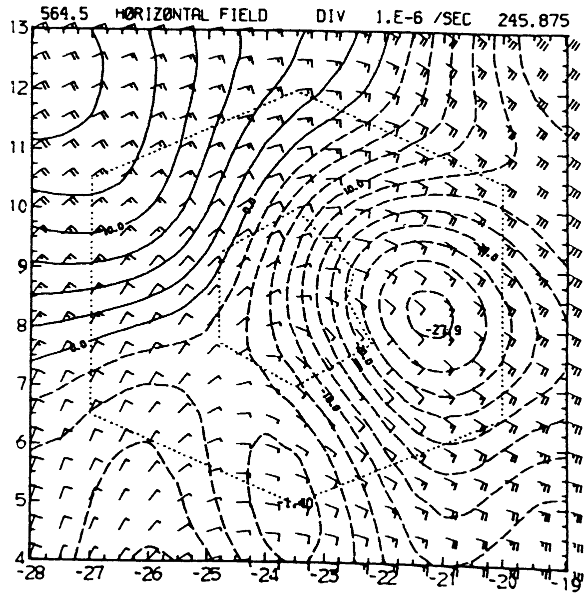

Figure 4. Horizontal cross-section of wind field and divergence at 565 hPa (near the freezing level) at 2100 UTC on day 245, showing peak convergence of 2.8 10^{-5} s^{-1}. The dotted lines are the GATE inner B-scale and outer A/B-scale ship arrays. Axes are latitude and longitude. Data is from Ooyama's analysis of GATE wind sounding data.

The evolution continues until by 2400 UTC, the residual circulation is a dipole mass field with ascent above the freezing level and descent below. Figure 4 is a horizontal cross-section from the same dataset of the divergence field at the freezing level at 2100 UTC, showing a large peak in the convergence at this level, centered near the location of our time-series of ω in Figure 3. This freezing level convergence associated with the mesoscale couplet of ascent over descent is as large an inflow as the low level convergence at any time in the cloud cluster lifecycle. An important question is whether this dipole circulation is well resolved by global models, or whether it should be parametrized as a heating-cooling couplet, which will then drive the dipole circulation in the large-scale model. We shall return to this later, as well as to the Cheng and Yanai [37] analysis of this case (in section 3.7), after discussing their diagnostic model.

3. Thermodynamic issues and diagnostic models

The second topic I shall review is the thermodynamic issues, which distinguish precipitating and non-precipitating convection. I will then discuss the key convective modes and finally outline the mass flux representation of deep convection used in diagnostic models, and some parametric models.

3.1 NON-PRECIPITATING CONVECTION

As long as cloud droplets are small, they are carried with air parcels. Reversible thermodynamics apply, provided there is no mixing; and ascent and descent of cloudy parcels follow saturated reversible adiabats [12] [4]. The enthalpy and water transports are well defined and well coupled to the mass flux, whether this is up or down. Indeed because the vertical motion is reversible, the net mass flux is enough to specify the net transports of enthalpy and water. However if non-precipitating parcels do not mix, their ascent and descent paths are identical, and net mass transports would be very small. The shallow convection process we see in the atmosphere is characterized by an essential irreversibility, caused by mixing between cloudy air parcels and their unsaturated and stably stratified environment. Cloudy parcels originating below cloud base, if they mix with air from above cloud base, which has a higher potential temperature, θ, as well as being unsaturated, cannot descend back as far as they ascended. Consequently the lifecycle of shallow clouds impose irreversible transports. Liquid water, which is condensed in the lower part of the cloud layer, is transported upwards and evaporated at higher levels (Betts [13] [40]), resulting in a couplet of convective cooling at the inversion layer over warming below (with no integrated enthalpy source, if the clouds do not precipitate). The mixing process, although irreversible, can however be treated to sufficient accuracy using conserved variables and mixing lines on a thermodynamic diagram (Betts [41]). In oceanic boundary layers (BL), the entire convective BL reaches an equilibrium between the convective transports, the subsidence and the radiation field, which is relatively easy to understand and model (for example Betts [40], Betts and Ridgway [42] [43]). The cloud field transports moist air with subcloud layer properties upwards in the face of mean subsidence. The upward transport of water by the clouds balances the drying effect of the mean subsidence; and the low liquid-water potential temperature, θ_L, of cloud air (initially the θ of the subcloud layer), together with longwave radiation, cools the warm air sinking through the inversion at BL-top. Because the whole layer equilibrium has closely a mixing line structure, and liquid water is carried with air parcels, the convective transports can be well represented by a single mass flux (Siebesma and Cuijpers [44]).

However once cloud droplets grow large enough to fall out of air parcels into unsaturated air, the cloud microphysics becomes important, and the entire thermodynamic picture becomes more complex.

3.2 PRECIPITATING CONVECTION AND THE LIMITATION OF MASS FLUX MODELS

Firstly, determining the fraction of the precipitation that falls out is important. θ_L is no longer conserved in the updrafts, and the subsequent thermodynamics of updraft parcels is different, as their cloud water is reduced considerably. Betts [45] proposed a simple pressure-scale parameterization for precipitation fallout, which gives asymptotic values for updraft cloud water. Even in small Trade-cumulus clouds, once they become deep enough to precipitate, the fallout of precipitation produces layering in the atmospheric structure. The reason is that downdrafts formed by the evaporation of rain penetrate vertically more than those formed by mixing; simply because, for the same change of mixing ratio q, virtual potential temperature, θ_v, changes faster along the moist adiabat (which is conserved in the evaporation of falling rain), than along typical shallow cumulus BL mixing lines, which constrain evaporation by mixing (Betts and Albrecht [46]). For evaporation driven downdrafts, the key thermodynamic issue is that only one air parcel parameter, θ_E, the equivalent potential temperature, is closely conserved in the evaporation process, and this does not determine the downdraft parcel subsaturation (unlike evaporation in a mixing process, when both θ_L and q_t and saturation pressure mix conservatively). By definition precipitation droplets are larger, they have a smaller surface to mass ratio, and they do not evaporate fast enough to keep the air into which they fall saturated, since this air, once cooled by evaporation, sinks in downdrafts, seeking a new level of buoyancy equilibrium. In this process, downdraft subsaturation is a result of an internal balance, which can be formulated conceptually in terms of a pressure scale for evaporation (Betts and SilvaDias [17]; Betts [45]).

$$\Pi_E = \rho g W_d \tau_E \qquad (1)$$

where W_d is a characteristic downdraft speed, and τ_E a characteristic evaporation time-scale for the water flux of the falling droplets, dependent in turn on their microphysical properties; mean size and number density. The significance of Π_E is that downdraft subsaturation, formulated in terms of the saturation pressure difference, $\mathcal{P}_d = p_d^* - p$ (where p^* is air parcel saturation pressure [41]), asymptotically approaches $-\Pi_E$ (see [17] [45]). For the simple case of a uniform population of N drops of size r, one can show (Kamburova and Ludlam [47], [17])

$$\tau_E = 4\pi D C_v N r \qquad (2)$$

where D is a coefficient of diffusion of water vapor in air, and C_v is a ventilation coefficient for the evaporation of falling drops. The rainfall rate, downdraft speed and negative buoyancy and the stratification are all interactive, but typically we observe in cumulonimbus downdraft outflows, subsaturations which correspond to values of Π_E from 35-120 mb, corresponding to low level relative humidities from 85-55%. In more unstable atmospheres

[17], where downdraft speeds are larger, we tend to see higher values of Π_E, corresponding to lower relative humidity

The key consequence of (1) is that, unlike moist updrafts, which remain close to saturation, the subsaturation of downdrafts depends on small-scale dynamical and microphysical parameters, which must be formulated in terms of large-scale model variables. This is in sharp contrast to the updraft circulation, which is very close to saturation (because the droplets are small and supersaturations are small, see for example Ludlam, [48]). Diagnostically if we measure downdraft inflow and outflow we can infer evaporation into them (e.g. Betts [15] [16]), but only a few parametric schemes (e.g. Emanuel [49], Betts and Miller [6]) have attempted to treat unsaturated downdrafts, even in a simple manner. Unfortunately in many convective parameterizations, moist downdrafts, if included at all, are formulated simply as a fraction of the updraft mass flux, and often treated as saturated. This successfully avoids the real complexity of the deep convective process by reducing the parametric problem to determining a single updraft mass flux, but it is an unsatisfactory simplification. ***Unlike shallow convection, deep convection is not a simple mass flux problem, because the precipitation is falling freely and interacting with the atmosphere.*** For *both* the updraft and downdraft circulations, only one variable θ_E is (approximately) conserved, and the submodels which handle the microphysics of precipitation fallout and evaporation into downdrafts are critical. The widespread use of mass flux models for cumulus parameterization has perhaps partially obscured this important issue. For precipitating convection, the true thermodynamics of *both* updraft and downdraft are poorly determined, because of this dependence on the microphysics. The updraft may be saturated (which gives the illusion of simplicity), but its cloud water (which determines its θ_L) is dependent on the microphysics. This is the reason Betts [45] proposed a symmetric parameterization using pressure scales for evaporation and the fallout of precipitation. Parallel to (1), one can relate a pressure scale for precipitation fallout, Π_F, to an updraft speed (W_u) and a timescale for the conversion of cloud water or ice to precipitation (τ_F)

$$\Pi_F = \rho g W_u \tau_F \tag{3}$$

The conversion timescale, τ_F, is of course not easy to estimate, as the underlying microphysics is complex, but the formulation is useful conceptually, because the saturation pressure difference $\mathcal{P}_u = (p_u^* - p)$ of a (hypothetical) steady-state updraft asymptotically approaches Π_F. Consequently, cloud water, ℓ_u, is also asymptotically related to Π_F [45]

$$\ell_u \to \Pi_F(\partial q_s/\partial p)_{\theta_{ES}} \tag{4}$$

For $\Pi_F \approx 50$ mb, $\ell \approx 1$ gKg^{-1} at warm temperatures. These two pressure scales (Π_F and Π_E) symbolically represent the key microphysical processes in convective updrafts and downdrafts, which essentially determine the saturation pressure of updraft and downdraft outflows.

3.3 THE IMPORTANCE OF THE SATURATION PRESSURE BUDGET

The saturation pressure (p^*) budget (see [41] [50] [51] [52]) is probably conceptually the second most useful budget for the study of precipitating convection, after the θ_E budget. It can be regarded as another combination of the temperature and humidity budgets with important conservation properties. For updrafts, saturation pressure difference, $\mathcal{P}$, is related to cloud water content. Expression (4) is a special case of

$$\ell_u = \mathcal{P}_u(\partial q_s/\partial p)_{\theta_{ES}} \tag{5a}$$

For downdrafts and the unsaturated environment, $\mathcal{P}$ is related to relative humidity (RH). For unsaturated air, a parallel relationship to (5a) exists

$$(q_w - q) = \mathcal{P}_u(\partial q_s/\partial p)_{\theta_{ES}} \tag{5b}$$

where q_w is saturation mixing ratio at the wet-bulb temperature [41], but a useful simple formulation of the direct relationship to RH is (see Appendix)

$$\mathcal{P} = p(1 - RH)/(A + (A-1)RH) \tag{6}$$

where the thermodynamic coefficient

$$A = \left(\frac{R}{R_v}\right)\left(\frac{L}{2C_pT}\right) \tag{7}$$

increases slowly with decreasing temperature. Substituting the ratio of the gas constants ($R/R_v = .622$), as well as the latent heat ($L = 2500$ JKg^{-1}) and specific heat of air ($C_p = 1006$ JK^{-1}Kg^{-1}) gives $A = 2.83$ at $T = 273$ K. (6) shows that ($\mathcal{P}/p$) and (1-RH) are closely related measures of subsaturation.

The vertical transport of water in the atmosphere is accomplished by clouds, and the outflows from convective systems. The transition at cloud boundaries, where the air is just saturated, and $p^* = p$, is in addition critical from the radiative perspective. The residual cloud water or ice in updraft outflows tends to bring the atmosphere closer to saturation (since $p_u^* > p$) in the upper troposphere, where mixtures tend to sink less far in the more stable stratification at these levels. The evaporation of falling precipitation produces unsaturated downdraft outflows in the lower troposphere. If pressure scales are used to parameterize the cloud microphysical processes controlling precipitation and evaporation in downdrafts, then these convective/microphysical pressure scales, together with the convective mass outflows (and large-scale advection), control the local saturation pressure budget of the atmosphere.

Outside cloud systems, adiabatic processes conserve saturation pressure, p^*, so that only the diabatic radiative process modifies p^* [46]. The equations in [46] contain errors, so a summary is given here. As air sinks with radiative cooling, we may write the time rate of change of $\mathcal{P}$ along trajectories as

$$\dot{\mathcal{P}} = \dot{p}^* - \omega \tag{8}$$

The right hand terms can both be related to the radiative cooling rate, $\dot{\theta}_R$. For saturation pressure

$$\dot{p}^* = \dot{\theta}_R/(\partial\theta/\partial p)_{q^*} \tag{9}$$

where the thermodynamic gradient is along lines of constant saturation mixing ratio q^*. For air parcel ω, a radiatively balanced subsidence rate is

$$\omega \approx \dot{\theta}_R / (\partial\bar{\theta}/\partial p) \qquad (10)$$

where the gradient is just the mean stratification. Typical values in the tropics just above the tradewind layer (600-800 mb) are $(\partial\bar{\theta}/\partial p) = -5K/100mb$ and $(\partial\theta/\partial p)_{q^*} \approx 12\,K/100mb$, so that

$$\omega > \dot{p}^* \qquad (11)$$

and as air parcels outside clouds sink in the free troposphere with radiative cooling, they become more unsaturated, because $\dot{\mathcal{P}} = (\dot{p}^* - \omega) < 0$. At 700 mb, with $\dot{\theta}_R \approx -1.75$ K day^{-1}, subsaturation increases at a rate $\dot{\mathcal{P}} \approx -20$ mb day^{-1}. The subsaturation of air in the subsiding branches of atmospheric circulations, which is an important radiative control on the climate in the tropics [43], [53] is thus linked to the mass circulation, and the time air has subsided with radiative cooling after crossing a cloud boundary.

3.4 THE FREEZING LEVEL

The freezing level is important in the tropics: it is in the middle troposphere near 550 mb. Usually it is the level where the thermal profile changes from unstable in saturation equivalent potential temperature, θ_{ES}, to stable [41]. Often there is a visible kink in the thermal θ_{ES} structure, and typically the level of minimum θ_E is near the freezing level. This has been known for many years, but it was not explicitly incorporated as a feature in a convective parameterization scheme until Betts [54], Betts and Miller [55]. Undoubtedly the stratiform precipitation phase change plays a role in the maintenance of this characteristic structure. We have already mentioned in section 2, that in the decay phase of convective mesosystems, the inflow peaks at the freezing level (Figure 4) with ascending motion above, and descending motion below. We shall discuss this convective mode further in section 3.5, and the relationship of the mid-tropospheric θ_E minimum to the upward θ_E flux in section 3.6.

3.5 THE KEY CONVECTIVE MODES

An important paper by Johnson [34] showed one method of partitioning diagnostic heat and moisture budgets into cumulus and mesoscale components. He assumed that the condensation in the mesoscale anvils was a certain fraction (≈0.2) of the total precipitation, and then derived the characteristic mesoscale couplet signature of the warming and drying above the freezing level and cooling and moistening below.

This paper was followed by a review by Arakawa and Chen [56] which contained some significant diagnostic insights. They distinguished different types of closure assumptions in parameterization schemes. In particular, they defined a Type II closure as one that constrained the coupling of the convective heat source $(Q_1\text{-}Q_R)$ and moisture sink (Q_2), using the notation of Yanai et al. [12], in which Q_1 is the total diabatic source term, and Q_R is the radiative contribution to this term. They used canonical correlation analyses on the GATE Phase III data [of Ooyama, Chu and Esbensen] and an Asian data set (from He et al. [57]) to show there were three principal modes of coupling of $(Q_1\text{-}Q_R)$ and Q_2. We show them schematically in Figures 5a, and 5b. Mode 1 is the principal deep convection mode associated with cumulonimbus updrafts and downdrafts through the deep troposphere. (We will associate their third mode with a modulation of Mode 1: see below). Since there is

heating throughout the atmosphere and net precipitation, this mode is associated with a single cell of mean upward vertical motion in the troposphere, although within that there are

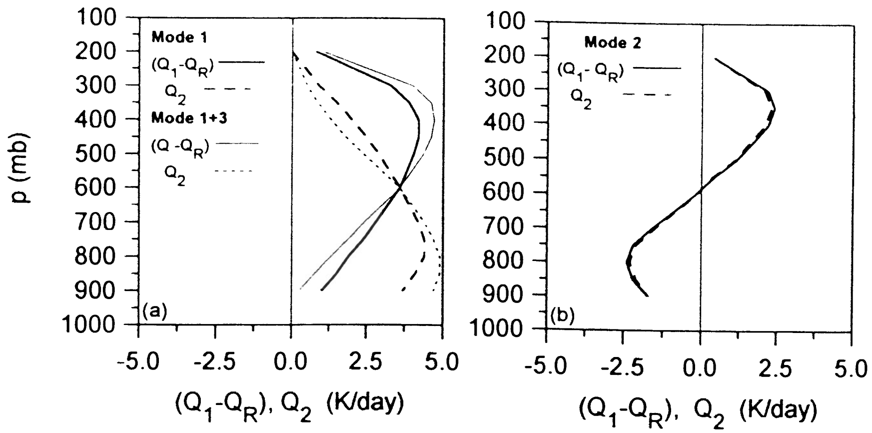

Figure 5. Modes of interaction of convective heating $(Q_1\text{-}Q_R)$ and drying (Q_2), freely adapted from Arakawa and Chen [1987]. Panel (a) shows modes 1 and 3; panel (b) is mode 2.

moist updrafts and downdrafts. There is a net upward flux of θ_E, peaking in the mid-troposphere, where the $(Q_1\text{-}Q_R)$ and Q_2 curves cross (see (13)). Mathematically, integrating over the troposphere (Yanai et al. [12] Betts [22]), and neglecting the surface sensible and latent heat fluxes, the surface precipitation flux $F_{PR}(0)$ is given by integrals of the convective source terms. For notational brevity, we use height rather than pressure co-ordinates and do not include density, which varies with height.

$$LF_{PR}(0) = \int_0^{z_T} (Q_1 - Q_R)\,dz = \int_0^{z_T} Q_2\,dz \qquad (12)$$

where z_T is a level high in the atmosphere, where the convective source terms are small.

There is a net upward transport of θ_E and moist static energy h associated with this mode since $Q_1 - Q_R < Q_2$ at low levels, given by [12]

$$(C_p T/\theta_E)\,F_{\theta_E}(z) \approx F_h(z) = -\int_0^{z_T} (Q_1 - Q_2 - Q_R)\,dz \qquad (13)$$

Arakawa and Chen [56] describe their third mode, as one which increases the separation of the Q_2, $Q_1 - Q_R$ peaks in Figure 5a. This Mode 3 has been drawn on Figure 5a as a modulation of Mode 1, which *increases* the mid-tropospheric θ_E flux, while having little impact on net precipitation. Thus this key diagnostic study shows that the upward θ_E flux is ***not uniquely*** coupled to the precipitation. Conceptually one might perhaps associate a larger upward θ_E flux with a dynamical structure which feeds more low θ_E air into the system in mid-levels.

In terms of the feedback to the larger scale, the net precipitation is important, because it is associated with heating and a deep tropospheric ascent mode. The importance of the upward θ_E flux is that this lowers boundary layer θ_E [15] [16] [22], and increases the ocean surface θ_E flux (primarily the moisture fluxes are involved). The importance of this process in regulating convection is discussed in detail by Raymond [58] [59].

The mode 2 in Figure 5b is described by [56] as the component representing deviations of "large-scale" condensation and evaporation, since $(Q_1 - Q_R) \approx -Q_2$ for this mode. Note that, as we have drawn it in Figure 5b, it represents a condensation over evaporation couplet with no net precipitation and zero θ_E flux (from Equations (3) and (4)). This diagnostically derived mode can be thought of as the signal coming from the variable presence of mesoscale anvils. The key consequence of this heating over cooling couplet (which in reality involves condensation and freezing over evaporation and melting) is to force a 2-cell vertical structure with ascent over descent, and a larger-scale convergence in mid-levels near the freezing level as seen in Figure 4.

In the light of this diagnostic study, which is consistent with our GATE September 2 GATE example, and those shown in Johnson [34], I propose that the minimum requirements for a convective parameterization scheme is whether it can represent these 3 idealized modes correctly.

a) A deep convective precipitating mode with an upward θ_E flux, not uniquely coupled to the precipitation (Modes 1 and 3)

b) A heating/cooling couplet with no net precipitation and no θ_E flux (Mode 2).

A scheme would then need sufficient closures to be able to determine the magnitude of the net precipitation, θ_E flux, and the heating over cooling couplet; and preferably their time evolution for an evolving unresolved mesoscale convective system.

One immediate question is does the couplet Mode 2 have to be parameterized at all? If it is "large-scale" precipitation, why can't the grid-scale processes handle it (provided there is an adequate prognostic cloud-scheme being fed liquid and solid precipitation from the convective scale)? We are approaching the heart of the so-called scale-interaction problem. What scales are well represented by the large-scale model? It is clearly unreasonable to expect a hydrostatic global climate model with a horizontal grid of 250 km to represent the mesoscale at all, but can a hydrostatic model with a 50 km grid develop a crude representation of a mesoscale anvil? The key test I would propose is whether the mid-level convergence, shown in Figure 4, develops in tropical convective systems in the model. If not, I would argue it should be forced by parametrically representing the Mode 2 couplet. In section 4.3, a simple formulation will be proposed.

From an observational perspective, what we see in the GATE data is that, while convective bands initially develop in favorable regions of large-scale waves, and therefore might be regarded as a response to large-scale destabilization, the subsequent convective and mesoscale developments control the evolution of the mass field. In nature, all the scales interact dynamically and can evolve together; but the convective and mesoscales have shorter time scales than certainly the rotational large-scale fields (although the convection is quite tightly coupled to the divergent field). Because we only simulate the dynamics of the large-scale in our global models, ***the faster processes must be parameterized.*** Just as a convection scheme, by introducing precipitation before saturation on the grid-scale is reached, can change the phasing of large-scale dynamical development, so if we introduce a parameterized mesoscale couplet forcing, this too will feed back on the large-scale model dynamics sooner, than if we wait for grid-scale processes to reach saturation. Since we know that this inflow at the freezing level is dynamically important in the tropics, it is likely that the impact of this Mode 2 parameterization will be significant.

3.6. MASS FLUX REPRESENTATION OF DEEP CONVECTIVE UPDRAFTS AND DOWNDRAFTS

There have been many discussions of the mass flux representation of cumulus transports following Yanai *et al.* [12] including papers by Johnson [60], Cho [61], Nitta [62], McBride [63], Arakawa and Chen [56], Cheng [35] [36] and Cheng and Yanai [37] and many others. For this review only a condensed summary will be given to illustrate the key issues. The subgrid-scale heating and drying by convective updrafts and downdrafts can be written in bulk form as

$$(Q_1 - Q_R) = -\frac{\partial F_{PR}}{\partial z} - \frac{\partial}{\partial z}[M_u(s_{Lu} - \bar{s})] + \frac{\partial}{\partial z}[M_d(s_d - \bar{s})] \qquad (14)$$

$$-Q_2 = \frac{\partial F_{PR}}{\partial z} - \frac{\partial}{\partial z}[M_u(q_{Tu} - \bar{q})] + \frac{\partial}{\partial z}[M_d(q_d - \bar{q})] \qquad (15)$$

We define the terms as follows. The updraft and downdraft mass fluxes are M_u, M_d respectively (both defined as positive), and they satisfy mass conservation equations

$$\partial M_u / \partial z = \epsilon_u - \delta_u \qquad (16)$$

$$-\partial M_d / \partial z = \epsilon_d - \delta_d \qquad (17)$$

where ϵ, δ represent entrainment and detrainment rates. The bulk properties of the updraft are its liquid water static energy s_{Lu} and total water q_u ; the downdraft is assumed to have no cloud water, so its properties are s_d, q_d. The environmental mean with properties $\bar{s}\,\bar{q}$ is also assumed unsaturated. We ignore large-scale horizontal advection of condensate. $F_{PR}(z)$ is the flux of precipitation, which is related to 3 terms

$$-\partial F_{PR} / \partial z = C_u - E_d + Q_M \qquad (18)$$

where C_u is the fallout of precipitation from the updraft, and E_d is the evaporation of falling precipitation into the downdraft. Following Arakawa and Chen [56] and Cheng and Yanai [37], and the schematic in Figure 5b, we include, in addition to the convective terms, a mesoscale condensation/evaporation couplet term, Q_M, (which is considered separately from the convective scale mass circulation), and which has both zero moist static energy (h) flux and no net precipitation flux. Thus Q_M satisfies the constraints

$$Q_M = Q_{1M} = Q_{2M} \qquad (19a)$$

and

$$\int_0^{z_T} Q_M \, dz = 0 \qquad (19b)$$

In (14) and (15) we have also not included for brevity the surface sensible and latent heat fluxes or any representation of 'turbulent' boundary layer fluxes.

From energy conservation in the updraft, which entrains and detrains, and condenses precipitation as it ascends, one can write the updraft budget equation

$$\frac{\partial}{\partial z}(M_u s_{Lu}) = C_u + \epsilon_u \bar{s} - \delta_u s_{Lu} \quad (20)$$

Similarly for the downdraft

$$\frac{\partial}{\partial z}(M_d s_d) = E_d + \epsilon_d \bar{s} - \delta_d s_d \quad (21)$$

where, in both (20) and (21), it is assumed that air entrained into both updraft and downdraft has the properties of the mean environment. Substituting (20) and (21) in (14) and (15), using (16), (17), and (18), and rearranging, gives

$$Q_1 - Q_R = M_c\, \partial\bar{s}/\partial z + \delta_u(s_{Lu} - \bar{s}) + \delta_d(s_d - \bar{s}) + Q_M \quad (22)$$

$$Q_2 = M_c \partial\bar{q}/\partial z + \delta_u(q_{Tu} - \bar{q}) + \delta_d(q_d - \bar{q}) - Q_M \quad (23)$$

where the net convective mass flux is

$$M_c = M_u - M_d \quad (24)$$

The equations (22) and (23) are the heart of many diagnostic studies of convection, and the parametric mass flux representation. Many of the authors cited above have used a spectral representation of the convective transports, but the bulk representation here is sufficient to illustrate the key issues, since the magnitudes (and the mechanisms) of the entrainment and detrainment terms are poorly known. Note that the convective updraft and downdraft mass fluxes can be formally combined in the leading terms, which have often been described in the literature as "compensating" subsidence terms. They are the terms which represent the bulk heating and drying by deep convection. The physical reality is that the mean grid scale ascent, $\overline{M}$, is simply carried upward on small scales as a net transport within convective towers (Riehl and Malkus [64]), that is $M_c \approx \overline{M}$, and the environmental motion between deep convective towers is small.

Cho [61] recognized that if the convective outflows are considered to be at buoyancy equilibrium, after evaporating any remaining cloud water (note that this depends on the precipitation parameterization), then one can formally drop the detrainment terms in (22) (if virtual temperature effects are neglected), and calculate an M_c from (also dropping the mesoscale term)

$$Q_1 - Q_R = M_c \partial\bar{s}/\partial z \quad (25)$$

It could be argued that this is a satisfactory treatment, except near the surface, where cold downdraft outflows cannot sink to buoyancy equilibrium. However Cho noted, that even if M_c is calculated from (25), there is no equivalent condition to buoyancy equilibrium in the moisture budget. The moisture content of convective outflows must be determined in (23) to solve the parameterization problem, since it cannot be assumed that $q_{Tu} = q_d = \bar{q}$. Downdraft outflows are typically unsaturated and must be modeled. The precipitation fallout determines the water content of updraft outflows, which, if they are negatively bouyant after evaporating their condensate, will be unsaturated after sinking to buoyancy equilibrium [41].

The net vertical mass transport of the deep convective mode is directly related to the net precipitation. Integrating (25) gives

$$\int_0^{z_T}(Q_1 - Q_R)dz = \int_0^{z_T}(M_c \partial\bar{s}/\partial z)dz \quad (26)$$

Substituting (18) in (14) and integrating through the troposphere gives

$$\int_0^{z_T}(Q_1 - Q_R)dz = F_{PR}(0) = \int_0^{z_T}(C_u - E_d)dz \quad (27)$$

since the convective fluxes disappear at the integration limits, and the mesoscale term disappears using (19b). (If we had not dropped the surface sensible heat flux it would also be included here) $F_{PR}(0)$ is again the surface precipitation flux. Thus (26) and (27) show that the deep mode with net precipitation is formally related to a net deep convective mass flux

If we add (22) and (23), the mesoscale term, which has no h transport because of (19a), again disappears and we get

$$Q - Q_2 - Q_R = M_c \frac{\partial\bar{h}}{\partial z} + \delta_u h_u' + \delta_d h_d' \quad (28)$$

where $h_u' = h_u - \bar{h}$, and $h_d' = h_d - \bar{h}$ In Betts [15], the inflows and outflows were measured directly and the terms in (28), including separate updraft and downdraft mass fluxes were evaluated. As mentioned earlier, at low levels, where M_c is small, the right hand side is dominated by the outflows of unsaturated downdraft air (since it was assumed that the inflow to the updraft had environmental mean properties, only the outflows appear in (19)). In other diagnostic studies using sonde networks to derive $Q_1 - Q_2$ (Q_R is usually calculated), (28) cannot be inverted by itself as it contains 2 unknowns, the updraft and downdraft mass fluxes. Only if downdrafts are neglected, can (28) be immediately inverted, given a cloud model for h_u, to derive a net convective mass flux M_c [12]. In some other diagnostic studies, the ratio of downdraft to updraft mass fluxes has been prescribed (e.g. Johnson [60]) to solve (28). Any two of (22), (23) and (28) can however be regarded as independent. Nitta (62) showed that, if a precipitation parameterization is introduced to determine the remaining cloud water in s_{Lu}' in (22), and the downdrafts are assumed to be saturated, then (22) and (28) can be solved simultaneously for both an updraft and downdraft mass flux.

The key conclusion is that the mass flux representation of convection is only adequate to the extent that the detrainment terms in (22) and (23) can be either neglected or calculated. In the middle troposphere, the vertical mass flux terms do dominate, but as pointed out in Betts [15], near the surface, the low level cooling and drying by convection depends essentially on downdraft outflows. Thus a satisfactory mass flux parameterization for deep convection must calculate both an updraft and a downdraft mass circulation and the properties of the outflows of both the updrafts and downdrafts. All these depend on microphysical and cloud-scale dynamical processes, so a satisfactory general solution has not yet been found.

Convective precipitation is linked to a convective mass flux (see (26) and (27)), but this alone does not determine the upward θ_E flux, which is also linked to the environmental θ structure, and the convective-scale dynamics. Combining (18) and (28), consider the integral to the freezing level z_F in the mid-troposphere

$$(C_p T/\theta_E)F_{\theta_E}(z_F) = F_h(z_F) = -\int_0^{z_F} M_c \frac{\partial\bar{h}}{\partial z}dz - \int_0^{z_F}\delta_u h_u' dz - \int_0^{z_F}\delta_d h_d' dz \quad (29)$$

At the freezing level, $\bar{h}$ is typically a minimum, so below z_F, $\partial\bar{h}/\partial z$ is negative, and the first term is positive. The downdraft outflows have typically h_d' negative, so the third term is also positive. If we neglect updraft outflows in the lower troposphere (which means ignoring shallow clouds), it is clear that the strength of mid-tropospheric upward deep convective flux of h (and θ_E) is related to the net convective mass flux, the value of the $\bar{h}$ minimum, and the strength and properties of the downdrafts. Since downdrafts bring down mid-tropospheric low $\bar{h}$ air, a low value of mid-tropospheric $\bar{h}$ contributes in both terms to a larger upward h flux. It is this upward flux of h or θ_E which plays a key role in the convective interaction with the surface fluxes as discussed earlier (see also Raymond [59]).

3.7 DIAGNOSTIC RETRIEVAL OF MESOSCALE SOURCE TERMS

Arakawa and Chen [56] and Cheng and Yanai [37] discussed a method of extracting the mesoscale flux information from (22) and (23). They defined a parameter $\boldsymbol{H}$, as follows, so as to eliminate the convective mass flux M_c.

$$\frac{\boldsymbol{H}}{(-L\partial\bar{q}/\partial z)} = \frac{Q_2}{(-L\,\partial\bar{q}/\partial z)} - \frac{(Q_1-Q_R)}{\partial\bar{s}/\partial z}$$
$$= -\left(\frac{\delta_u q_{Tu}' + \delta_d q_d'}{-L\partial\bar{q}/\partial z}\right) - \left(\frac{\delta_u s_{Lu}' + \delta_d s_d'}{\partial\bar{s}/\partial z}\right) + Q_M\left(\frac{1}{-L\partial\bar{q}/\partial z} - \frac{1}{\partial\bar{s}/\partial z}\right) \qquad (30)$$

Cheng and Yanai argue that the detrainment terms are dominated by the detrainment of water from the updrafts ($\delta_u q_{Tu}'$): this term makes a negative contribution to $\boldsymbol{H}$. In contrast the mesoscale term can be rearranged as

$$\frac{Q_M\,\partial\bar{h}/\partial z}{(\partial\bar{s}/\partial z)\,(-L\,\partial\bar{q}/\partial z)} \qquad (31)$$

Since the typical mesoscale couplet has Q_M positive in the upper troposphere where $\partial\bar{h}/\partial z$ is positive, and negative in the lower troposphere where $\partial\bar{h}/\partial z$ is negative, this mesoscale term is positive at all levels. Cheng and Yanai [37] noticed that $\boldsymbol{H}$ was positive during GATE convective cluster episodes, so the mesoscale term must dominate over the negative convective scale detrainment term in these cases. They used a cloud model to calculate the detrainment terms, and successfully estimated the mesoscale heating/cooling couplet.

Figures 6a and 6b from Cheng and Yanai [37] show the results of their diagnostic model at 1800 UTC for the GATE Case Study on Day 245, which we discussed earlier in section 2.3. Figure 6a shows a cross-section of what they called the mass flux in the cumulus environment.

$$\tilde{M} = \bar{M} - M_c \qquad (32)$$

where $\bar{M}$ is the observed mean vertical mass flux and M_c is the net cumulus mass (updrafts and downdrafts) diagnosed by their model. In the presence of cloud clusters, the authors regarded $\tilde{M}$ as a measure of the mesoscale mass flux. Figure 6b is the corresponding cross-section of the mesoscale convective heating term, Q_M, found by subtracting the convective contribution (diagnosed by their model) from the total $(Q_1\text{-}Q_R)$, diagnosed from the sonde budget analysis. The characteristic heating over cooling couplet can be seen. Their longitude cross-section at 1800 UTC is along 8.5°N through the center of the GATE array. Note that

Figure 6a shows mesoscale ascent over descent at 1800 UTC, while the total mass flux at that time in Figure 3 (at 22°W) does not show descent in the lower troposphere. The diagnostic analysis leading to Figure 6 has however removed the convective mass flux. Figure 3 only shows the ascent over descent pattern later in the lifecycle of the convective system, presumably after the convective circulations have decayed further. It would be useful if the analysis of [37] could be repeated using other cloud models, since it is likely that their general conclusion is not cloud model dependent.

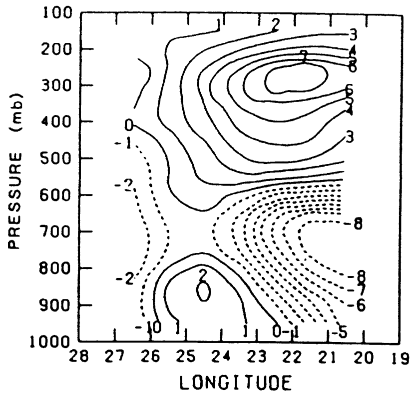

Figure 6a. Cross-section at 1800 UTC along 8.5°N, through center of the GATE ship array, of $\tilde{M}$ in mb hr^{-1}, a measure of the mesoscale mass circulation.

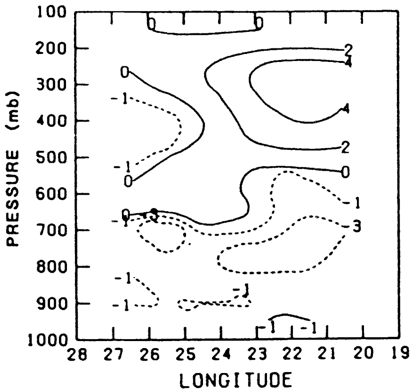

Figure 6b. As Fig 6a for the derived mesoscale heating Q_M (K day^{-1}).
(From Cheng and Yanai, 1989)

4. The Betts-Miller Scheme

4.1. BRIEF REVIEW

I will not outline the details of the Betts-Miller scheme here, as they are adequately covered in the recent review by [6], but the underlying concepts will be mentioned. It was clear in the decade after the GATE experiment, one of whose key objectives was to resolve the parameterization and 'scale-interaction' problem [1], that we had not found a simple solution. Some advocated more detailed cloud models [2] with hierarchies of convective and mesoscale updrafts and downdrafts, but it was clear that the key issue of closure, the linking of all the submodels to each other and to large-scale parameters, was unresolved. The Betts-Miller scheme [6][54][55] was one response to this. It is an attempt to formulate the convective forcing in a very simple mathematical way, so that perhaps the coupling can be explored in some detail. The idea was lagged convective adjustment towards convective equilibrium profiles of T and q. Since we see convection in the tropics adjust the atmosphere towards quasi-equilibrium structures, can we not directly model this process, perhaps more easily than trying to get it as an outcome of complex convection sub-models?

I introduced three concepts:

a) The moist virtual adiabat (the reversible adiabat), rather than the pseudoadiabat, as a reference adiabat up to the freezing level. This was an inference from observations. The scheme adjusts towards a thermal reference profile, which has a specified instability in the lower troposphere, defined with reference to this moist virtual adiabat

b) The freezing level was built into the parameterization in calculating the quasi-equilibrium reference profiles, because observationally it appeared to be significant. This was a recognition that the freezing-melting process also plays a role in determining the characteristic thermal structure with a θ_{ES} minimum

c) The adjustment was lagged, to represent the response time of the convective and mesoscales to changes on the large-scale. This gives a smoothed convective feedback, which seems physically more realistic than the on-off behavior of "instantaneous" convection schemes. In addition the mathematical structure allows the possibility of simplified analytical solutions (Neelin and Yu [65]). Indeed versions of this scheme have since proved useful in simple tropical climate models (Seager and Zebiak [66] [67]).

The key idea in this parameterization is that, while convection is occurring, the atmosphere is never allowed to get too far from the type of thermodynamic structures we observe. Even if we cannot adequately model the convective terms in detail, if we constrain a model in this way in the face of large-scale forcing, we are *imposing* the convective sources of heat and moisture, that we would derive by diagnostic methods.

In our later paper (Betts and Miller [6]), we introduced a unsaturated model downdraft circulation with its own adjustment time, based on a simple coupling of the evaporation into the downdraft to the net precipitation. This was an attempt to directly model unsaturated downdraft outflows into the boundary layer, and some improvements in the tropical climate resulted ([6], Slingo et al. [68]). In [55], the adjustment near the surface was not well constrained.

Even a decade after its introduction, this lagged adjustment approach still has validity, as we have yet to answer key questions of closure, and find ways of linking the dynamical and thermodynamic transports on all the unresolved scales (from individual cells to say the 50 km scale) to the scales resolved by global models. Two further extensions will now be proposed.

4.2. ADJUSTMENT TIME-SCALES FOR THE BETTS-MILLER SCHEME

Betts and Miller [6] present no theory for determining their convective adjustment time (τ), other than the empirical approach of setting τ short enough to make saturation on the grid scale infrequent. They recognized that this required smaller τ in higher resolution models as maximum values of grid-scale $\overline{\omega}$ increase. A simple dynamical basis for τ is proposed here. Elsewhere in this volume, Mapes [69] discusses the critical gravity-wave modes for the convection feedback to the large-scale. The first, a vertical wave-mode 1, spanning the deep troposphere has the fastest gravity wave propagation speed of 50 ms^{-1} (Table 1), while the second wave-mode 2, the dipole with a node at the freezing level, has a slower gravity wave speed ~25 ms^{-1} These are the two convective modes which interact rapidly with the larger scale flow. These are also the Modes 1 and 2 that we discussed in section 3.5, for which the diagnostic study of Arakawa and Chen [56] showed characteristic structure and transports. Consequently, using the phase speeds for these modes, one can estimate corresponding adjustment times for the Betts-Miller scheme. Table 1 shows values for three model grid lengths: 60 km, characteristic of the ECMWF forecast model (with spectral truncation of T-213); 120 km and 400 km, characteristic of a relatively low resolution climate model. This would give a formal basis for changing τ with horizontal resolution,

although again some empirical adjustment may be necessary

The adjustment time scales suggested by Betts and Miller [6] (1 hr at T-106, corresponding roughly to 120 km horizontal resolution) lie in between the values given for the fast Mode 1 and the slower Mode 2, suggesting that their empirical approach had some merit

TABLE 1 Adjustment times as a function of horizontal scale for two primary wave-modes.

	Wave-speed	Adjustment time τ		
	C(ms^{-1})	(60 km)	(120 km)	(400 km)
Wave-Mode 1 (Deep Troposphere)	50	20 min	40 min	2.2 hrs
Wave-Mode 2 (Inflow at Freezing Level)	25	40 min	80 min	4 4 hrs

However this heuristic dynamical model for τ does raise clearly a new issue. Gravity wave propagation can adjust quickly the thermal (buoyancy) structure on larger scales with these adjustment times. However it is not obvious that the moisture structure is adjusted on the same time scale, as is assumed in Betts and Miller [6]. This relates back to the discussion in section 3.6. Vertical displacements by gravity waves can simulate the thermal mass transport model represented by equation (25), but in the equivalent moisture equation the "detrainment terms" cannot be neglected. This needs further study

One unanswered question, which was raised in section 3.5, is whether convection parameterization schemes should have an explicit formulation of this wave-mode 2 forcing of the large-scale. One could argue that a global model with 60 km resolution, and an explicit cloud scheme, might possibly generate a marginal, but adequate representation of the stratiform precipitation and this mesoscale couplet on the grid-scale. However without the non-hydrostatic mesoscale dynamics, it may not. This could be explored numerically since the key feature, the development of the strong mid-level inflow in the mature and decaying phase of a mesoscale system, should be visible. Here we will argue the reverse: namely that only by improving the representation of a mesoscale wave-mode 2 couplet, linked to the convective-scale, will the convective forcing of the large-scale be adequately represented in most, if not all, hydrostatic global models In any event, this is a key scale separation issue, which needs exploring by a variety of techniques.

4.3 EXPLICIT PARAMETERIZATION OF MESOSCALE CONDENSATION-EVAPORATION COUPLET

We will illustrate this suggestion by proposing a simple extension to the Betts-Miller scheme (or any other convection scheme) to include a mesoscale precipitation-evaporation couplet. This is a further extension of Betts and Miller [6], who proposed a formulation for an unsaturated downdraft circulation, with its own time-scale linked to the precipitation. This idealized Mode 2 couplet has no θ_E transport, and no net precipitation, but does redistribute enthalpy by means of condensation/freezing aloft above evaporation/melting below. In the tropics the freezing level is almost half the pressure depth of the deep convective layer, so we can then represent the convective mesoscale forcing mechanisms shown schematically in Figure 5b, as a simple sine function in pressure coordinates

$$Q_M = \frac{C_p \partial T_M}{\partial t} = \frac{-L\partial q_M}{\partial t} = \frac{\pi L P_M}{(p_o - p_T)} \sin[2\pi(p - p_T)/(p_o - p_T)] \tag{33}$$

where p_o is the surface pressure, and p_T is the top of the deep convective layer This satisfies the constraints (19a) and (19b) (in pressure coordinates). We need to link this exchange to the net convective heating, so the simple closure is proposed

$$P_M = \beta F_{PR} \tag{34}$$

where F_{PR} is the surface precipitation rate, and the tunable parameter β is perhaps ≈0.2 (Johnson [34]). The magnitude of β effectively couples the adjustment time and amplitude of this mode to that of the deep convective mode. This mesoscale mode parameterization would be imposed in addition to the convective parameterization. It does not affect the net precipitation or vertical θ_E transport, but it does change the vertical redistribution of enthalpy and water. The issue of the lifecycle of mesoscale systems has still not been addressed. In climate models in which the resolved horizontal scale is larger, one might plausibly argue that within one model grid cell, large enough to include several convective mesosystems, that the simultaneous representation of convective and mesoscale components is adequate. In higher resolution forecast models, this may not be satisfactory, and some means of representing convective system lifecycles may still be needed. Indeed, since the evolution of many of the GATE mesoscale systems also appeared to be linked to the diurnal cycle, further work on this is needed.

5. Summary

This paper summarizes some important concepts in the parameterization of shallow and deep convection in large-scale numerical models. Starting in the early 1970's, diagnostic models have influenced the development of cumulus parameterizations, and field programs in the tropics, such as VIMHEX and GATE, showed the complexity of the life-cycle evolution of mesoscale systems with convective and mesoscale updrafts and downdrafts, coupled to the condensation and evaporation process. It is important to appreciate the thermodynamic differences between nonprecipitating and precipitating convection. Shallow, non-precipitating convection can be modeled using a mass transport model, and any two independent conserved variables (or alternatively using convective adjustment to quasi-equilibrium convective structures). Ironically, despite its simplicity and its key role in controlling the surface fluxes both over the ocean and over land, we have yet to parameterize shallow convection satisfactorily in numerical models. In contrast, precipitating convection is much more complex and difficult to parameterize. Precipitation falls from updrafts and evaporates driving downdrafts, so θ_L is not conserved. Only the θ_E flux depends on the updraft and downdraft mass fluxes. Cloud microphysics control precipitation, and in addition the downdraft thermodynamics is poorly known, as downdrafts remain unsaturated, with a subsaturation that depends on small-scale dynamical and microphysical balances. Consequently the θ_E flux is not tightly coupled to the enthalpy and water fluxes, which depend greatly on the precipitation flux, and its change with height through condensation and evaporation of falling precipitation. Diagnostic studies have shown that while the principal deep convective mode is tied to precipitation, and a deep tropospheric upward mass circulation, the upward θ_E flux, which interacts strongly with the subcloud layer over the oceans, is not uniquely coupled to the precipitation In addition, diagnostic studies show there is a key second convective mode associated with the mesoscale anvil couplet of ascent over descent, which might be parameterized in the same way as large-scale condensation, as a condensation-evaporation couplet without any θ_E transport or surface precipitation.

The concepts behind the Betts-Miller scheme are briefly reviewed, and two extensions are proposed. One is a theoretical basis for the adjustment time scale, based on the gravity wave propagation speed of the two primary modes. The second is a suggestion that the mesoscale couplet mode be explicitly parameterized, and coupled to the surface precipitation. Although this does not address the cloud cluster life cycle issue, which may matter in high resolution global models, or through coupling to the diurnal cycle, it might provide new insight into how these two convective modes interact with the large-scale flow

6. Acknowledgments

I was stimulated to write this work by the faculty and students of the NATO Advanced Study Institute at Kloster Seeon in August 1996. My research has been supported for many years by the National Science Foundation, currently under Grant ATM95-05018. I am grateful to Vic Ooyama for discussions in 1980, to Steve Esbensen for retrieving the data in Figure 3, and to Brian Mapes and Roger Smith for a thoughtful reviews.

7. References

1. Betts, A.K. (1974) The scientific basis and objectives of the U.S. Convection Subprogram for the GATE. *Bull. Amer. Meteor. Soc.*, **55**, 304-313.
2. Frank, W.M. (1983) The cumulus parameterization problem, *Mon. Weather Rev.*, **111**, 1859-1871.
3. Cotton, W.R. and R.A. Anthes (1989) Storm and Cloud Dynamics. Geophysics Series No. 44., Academic Press, San Diego, CA, 883pp.
4. Emanuel, K.A. (1994) Atmospheric Convection., Oxford University Press, New York, NY 588 pp.
5. Emanuel, K.A. and D.J. Raymond (1993) The Representation of Cumulus Convection in Numerical Models of the Atmosphere., *Amer. Meteor. Soc., Meteor. Mon.* **24**, No 46, 246pp.
6. Betts, A.K. and M.J. Miller (1993) The Betts-Miller scheme. Chapter 9 in *"The Representation of Cumulus Convection in Numerical Models of the Atmosphere"*. (Eds. K.A. Emanuel and D.J. Raymond.) *Amer. Meteor. Soc., Meteor. Mon.* **24**, No 46, 107-121
7. Kuo, H.L. (1965) On formation and intensification of tropical cyclones through latent heat release by cumulus convection. *J. Atmos Sci.*, **22**, 40-63.
8. Manabe, S., and R. Strickler (1965) Thermal equilibrium of the atmosphere with a convective adjustment. *J. Atmos Sci.*, **21**, 361-385.
9. Ooyama, K.V. (1969) Numerical simulation of the life cycle of tropical cyclones. *J. Atmos. Sci.*, **26**, 3-40.
10. Ooyama, K.V. (1971) A theory on parameterization of cumulus convection. *J. Meteor. Soc.*, **49**, 744-756.
11. Arakawa, A., and W. Schubert (1974) Interaction of a cumulus cloud ensemble with the large-scale environment, I, *J. Atmos. Sci.*, **35**, 674-701.

12. Yanai, M. S. Esbensen, and J.H. Chu (1973) Determination of bulk properties of tropical cloud clusters from large-scale heat and moisture budgets, *J. Atmos Sci.*, **30**, 611-627
13. Arakawa, A., and M-D. Cheng (1993) The Arakawa-Schubert Cumulus Parameterization, Chapter 10 in *"The Representation of Cumulus Convection in Numerical Models of the Atmosphere"* (Eds K.A Emanuel and D.J Raymond.) *Amer Meteor Soc., Meteor Mon* **24**, No 46, 123-136
14. Betts, A.K. (1973a) Non-precipitating cumulus convection and its parameterization. *Quart J R. Meteorol. Soc.*, **99**, 178-196.
15. Betts, A.K. (1973b) A composite cumulonimbus budget, *J. Atmos. Sci*, **30**, 597-610.
16. Betts, A.K. (1976) The thermodynamic transformation of the tropical subcloud layer by precipitation and downdrafts, *J. Atmos. Sci.*, **33**, 1008-1020.
17. Betts. A.K., and Silva Dias (1979) Unsaturated downdraft thermodynamics in cumulonimbus, *J. Atmos. Sci.*, **36**, 1061-1071
18. Miller, M.J., and A.K. Betts (1977) Travelling Convective Storms over Venezuela. *Mon. Wea. Rev.*, **105**, 833-848.
19. Zipser, E.J. (1969) The role of organized unsaturated convective downdrafts in the structure and rapid decay of an equatorial disturbance, *J. Appl. Meteorol.*, **8**, 799-814.
20. Zipser, E.J. (1977) Mesoscale and convective-scale downdrafts as distinct components of squall-line circulation, *Mon. Wea. Rev.*, **105**, 1568-1589.
21. Houze, R.A., Jr. (1977) Structure and dynamics of a tropical squall-line system observed during GATE, *Mon. Weather Rev.*, **105**, 1540-1567.
22. Betts, A.K. (1978) Convection in the tropics, in *Meteorology Over the Tropical Oceans*, pp. 105-132, Royal Meteorological Society, Bracknell, England.
23. Houze, R.A., and A.K. Betts (1981) Convection in GATE. *Rev. Geophys. and Space Phys.*, **19**, 541-576.
24. Leary, C.A., and R.A. Houze, Jr. (1979a) The structure and evolution of convection in a tropical cloud cluster, *J. Atmos. Sci.*, **36**, 437-457.
25. Leary, C.A., and R.A. Houze, Jr. (1979b) Melting and evaporation of hydrometeors in precipitation from the anvil clouds of deep tropical convection, *J. Atmos. Sce*, **36**, 669-679.
26. Leary, C.A., and R.A. Houze, Jr. (1980) The contribution of mesoscale motions to the mass and heat fluxes of an intense tropical convective system, *J. Atmos. Sce.*, **37**, 784-796.
27. Barnes, G.M. and K. Sieckman (1984) Mass inflow normal to fast and slow tropical mesoscale convective cloud lines. *Mon. Wea. Rev.*, **112**, 1782-1794.
28. Ooyama, K.V. (1987) Scale controlled objective analysis. *Mon. Wea. Rev.*, **115**, 2479-2506.
29. Esbensen, S.K., and K.V. Ooyama (1983) An objective analysis of temperature and relative humidity data over the B and A/B ship arrays during Phase III of GATE. Department of Atmospheric Sciences, Oregon State University, 87 pp.
30. Tollerud, E.I. and S.K. Esbensen (1985) A composite life-cycle of nonsquall mesoscale convective systems over the tropical ocean. Part I: Kinematic fields, *J. Atmos Sci.*, **42**, 823-837.
31. Esbensen, S.K., J-T Wang and E.I. Tollerud (1988) A composite life-cycle of nonsquall mesoscale coinvective systems over the tropical ocean. Part II: Heat and moisture budgets, *J. Atmos Sci.*, **45**, 537-548
32. Frank, W.M. (1978) The lifecycle of GATE convective systems. *J. Atmos. Sci.*, **35**, 1256-1264.
33. Johnson, R.H. (1980) Diagnosis of convective and mesoscale motions during Phase III of GATE. *J. Atmos. Sci.* **37**, 2399-2413.
34. Johnson, R.H. (1984) Partitioning tropical heat and moisture budgets into cumulus and mesoscale components: Implication for cumulus parameterization. *Mon. Wea. Rev.* **112**, 1590-1601.
35. Cheng, M.-D. (1989a) Effects of Downdrafts and Mesoscale Convective Organization on the Heat and Moisture Budgets of Tropical Cloud Cluster. Part I: A Diagnostic Cumulus Ensemble Model, *J. Atmos. Sci.*, **46**, 1517-1538.

36. Cheng, M.-D. (1989b) Effects of Downdrafts and Mesoscale Convective Organization on the Heat and Moisture Budgets of Tropical Cloud Cluster Part II Effects of Convective-Scale Downdrafts *J. Atmos Sci*, **46**, 1540-1564
37. Cheng, M.-D. and M Yanai (1989) Effects of Downdrafts and Mesoscale Convective Organization on the Heat and Moisture Budgets of Tropical Cloud Cluster Part III Effects of Mesoscale Convective Organization, *J. Atmos. Sci*, **46**, 1566-1488.
38. Mower, R.N., G.L. Austin, A.K. Betts, C. Gautier, R. Grossman, J. Kelley, F. Marks, and D.W. Martin (1979) A case study of GATE convective activity, *Atmos. Ocean*, **17**, 46-59
39. Warner, C (1980) Cloud measurements on day 245 of GATE, *Atmos. Ocean*, **18**, 207-226.
40. Betts, A.K. (1975) Parametric interpretation of trade-wind cumulus budget studies. *J. Atmos Sci.*, **32**, 1934-1945.
41. Betts, A.K., (1982a) Saturation point analysis of moist convective overturning *J. Atmos Sci*, **39**, 1484-1505.
42. Betts, A.K. and W. Ridgway (1988) Coupling of the radiative, convective and surface fluxes over the equatorial Pacific. *J. Atmos. Sci.*, **45**, 522-536.
43. Betts, A.K. and W. L. Ridgway (1989) Climatic equilibrium of the atmospheric convective boundary layer over a tropical ocean. *J. Atmos. Sci.*, **46**, 2621-2641
44. Siebesma, A.P., and J.W.M. Cuijpers (1995) Evaluation of parametric assumptions for shallow cumulus convection, *J. Appl. Meteorol.*, **52**, 650-666.
45. Betts, A.K. (1982b) Cloud thermodynamic models in saturation point coordinates. *J. Atmos Sci.* **39**, 2182-2191
46. Betts, A. K., and B. A. Albrecht (1987) Conserved variable analysis of boundary layer thermodynamic structure over the tropical oceans. *J. Atmos. Sci.*, **44**, 83-99.
47. Kamburova, P.L. and F.H. Ludlam (1966) Rainfall evaporation in thunderstorm downdrafts. *Quart. J. Roy. Meteor. Soc.*, **92**, 510-518.
48. Ludlam, F.H. (1980) Clouds and Storms. Pennsylvania State Univ. Press, Univ. Park, PA, 405pp.
49. Emanuel, K.A. (1991) A scheme for representing cumulus convection in large-scale models, *J. Atmos. Sci.*, **48**, 2313-2335.
50. Betts, A. K., (1984) Boundary layer thermodynamics of a High Plains severe storm. *Mon. Wea.Rev.*, **112**, 2199-2211
51. Betts, A.K., 1992: FIFE Atmospheric Boundary Layer Budget Methods. *J.G.R.*, **97**, 18523-18532.
52. Betts, A.K. and J.H. Ball, (1995) The FIFE surface diurnal cycle climate. *J.G.R.*, **100**, 25679-25693.
53. Pierrehumbert, T.T (1995) Thermostats, radiator fins and the local runaway greenhouse. *J. Atmos. Sci.*, **52**, 1784-1806.
54. Betts, A. K., (1986) A new convective adjustment scheme. Part I: Observational and theoretical basis. *Quart. J. Roy. Meteor Soc*, **112**, 677-692.
55. Betts, A. K. and M. J Miller, (1986) A new convective adjustment scheme. Part II Single column tests using GATE-wave, BOMEX, ATEX, and Arctic Airmass data sets. *Quart. J. Roy. Meteor. Soc.*, **112**, 693-710.
56. Arakawa, A., and J.-M. Chen (1987) Closure assumptions in the cumulus parameterization problem. *Short- and Medium-Range Numerical Prediction*, Collection of papers presented at the WMO/IUGG NWP Symposium, Tokyo, T. Matsuno, Ed., *Meteor. Soc Japan*, 107-131
57. He H., J.W. McGinnis, Z Song, and M. Yanai (1987) Onset of the Asian Summer Monsoon in 1979 and the Effect of the Tibetan Plateau, *Mon. Weather Rev.*, **115**, 1966-1995
58. Raymond, D.J. (1995) Regulation of moist convection over the west Pacific warm pool, *J. Atmos. Sci.*, **52**, 3945-3959.
59. Raymond, D.J. (1996) Boundary layer quasi-equilibrium. (This Volume).
60. Johnson, R.H. (1976) The role of convective-scale precipitation downdrafts in cumulus and synoptic scale interactions, *J. Atmos. Sci.*, **33**, 1890-1910.

61 Cho, H.-R. (1977) Contribution of cumulus cloud life-cycle effects to the large-scale heat and moisture budget equations, *J. Atmos. Sci.*, **34**, 87-97
62 Nitta, T (1977) Response of cumulus updraft and downdraft to GATE A/B-scale motion systems, *J. Atmos. Sci.*, **34**, 1163-1186.
63. McBride, J.L. (1981) An analysis of diagnostic cloud mass flux models. *J. Atmos Sci*, **38**, 1977-1990.
64 Riehl, H., and J S. Malkus (1958) On the heat balance of the equatorial trough zone. *Geophysica*. **6**, 503-538.
65. Neelin, J.D. and J-Y Yu (1994) Modes of tropical variability under convective adjustment and the Madden-Julian oscillation. Part I: Analytical theory. *J. Atmos Sci.*, **51**, 1876-1894.
66. Seager, R. and S.E. Zebiak (1995) Simulation of tropical climate with a linear primitive equation model. *J. Climate* **8**, 2497-2520.
67 Seager, R. and S.E. Zebiak (1996) Coupling between clouds, radiation, convection and surface fluxes in a tropical climate model. Submitted to *Mon. Wea. Rev.*
68. Slingo, J., M. Blackburn, A. Betts, R. Brugge, B. Hoskins, M. Miller, L. Steenman-Clark, and J. Thuburn, (1994) Mean climate and transience in the tropics of the UGAMP GCM. Part I: Sensitivity to convective parametrization., **120**, 861-880.
69. Mapes, B.E. (1996) Mutual adjustment of mass flux and stratification profiles (This volume).

Appendix. Relation between relative humidity and $\mathcal{P}$

The relation between saturation pressure difference $\mathcal{P}$ and RH is of some interest, because $\mathcal{P}$ is more directly related than RH to vertical circulations and convective processes in the atmosphere (see 3.3). Consider an unsaturated parcel at (p,T) with vapor pressure e, saturation vapor pressure e_s, lifted adiabatically to its saturation pressure p^*. Consider the linearization between p and p^*, along the dry adiabat θ and line of constant mixing ratio q, shown in Figure A1.

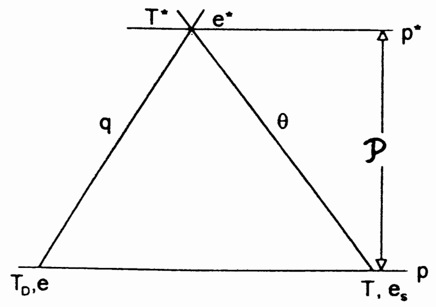

Figure A1. Schematic thermodynamic diagram showing paths of temperature, dewpoint and the corresponding vapor pressures of an unsaturated parcel lifted to saturation.

$$(e_s - e) = \mathcal{P}\left[\left(\frac{\partial e_s}{\partial p}\right)_\theta - \left(\frac{\partial e}{\partial p}\right)_q\right] \tag{A1}$$

On a line of constant mixing ratio q, e changes only slowly with pressure, and

$$\left(\frac{\partial e}{\partial p}\right)_q = \frac{e}{p} = \frac{e^*}{p^*} = \text{constant} \tag{A2}$$

On the dry adiabat, e_s changes rapidly. Expanding and using Clausius-Clapyron gives

$$\left(\frac{\partial e_s}{\partial p}\right)_\theta = \left(\frac{de_s}{dT}\right)\left(\frac{\partial T}{\partial p}\right)_\theta = \left(\frac{Le_s}{R_v T^2}\right)\left(\frac{RT}{C_p p}\right)$$

$$= \left(\frac{R}{R_v}\right)\left(\frac{L}{C_p T}\right)\left(\frac{e_s}{p}\right) \tag{A3}$$

Although in A3, (e_s/p) varies strongly from p to p^* on constant θ, we can linearize between the saturation point (where $e^*/p^* = e/p$, using (A2)) and e_s/p at pressure p, and to good approximation also neglect the variation of $1/T$. Doing this, A1 simplifies to

$$(e_s - e) = \frac{\mathcal{P}}{p}\left[\left(\frac{R}{R_v}\right)\frac{L}{C_p T}\left(\frac{e_s + e}{2}\right) - e\right] \tag{A4}$$

Defining $RH = e/e_s$, and $2A = \left(\frac{R}{R_v}\right)\left(\frac{L}{C_p T}\right)$ gives, on rearrangement, equation (6)

$$\mathcal{P} = p(1 - RH)/(A + (A-1)RH) \tag{6}$$

The thermodynamic coefficient, A, increases with decreasing temperature from 2.6 at 25°C to 3.4 at -40°C. (6) is quite accurate: it gives $\mathcal{P}$ to ≤ 1 mb for RH>0.5 and p>200 mb.